

## Evaluation of Correlations of Flow Boiling Heat Transfer of R600a in a Flat-Plate Solar Collector/Evaporator

William Quitiaquez<sup>a,\*</sup>, Eduardo Cortez<sup>a</sup>, Karen Anchaxi<sup>a</sup>, C.A. Isaza-Roldán<sup>b</sup>, César Nieto-Londoño<sup>b</sup>, Fernando Toapanta-Ramos<sup>a</sup>

<sup>a</sup> Universidad Politécnica Salesiana, Quito, Pichincha, 170108, Ecuador

<sup>b</sup> Universidad Pontificia Bolivariana, Medellín, 050031, Colombia

Corresponding author: \*wquitiaquez@ups.edu.ec

**Abstract**— In the current research work, the behavior of the boiling heat transfer coefficient in a flat-plate solar collector/evaporator, component of a direct-expansion solar-assisted heat pump (DX-SAHP) was studied using a hydrocarbon refrigerant with zero Ozone Depletion Potential (ODP) and low Global Warming Potential (GWP). The main dimensions of the collector/evaporator are 0.8, 3.8, and 1000 mm of the fin thickness, internal diameter, and length, respectively. Five experimental tests were realized at different times of the day for obtaining the results, with mass velocities varying between 197.59 and 267.26 kg·m<sup>-2</sup>·s<sup>-1</sup>, and the heat flux having values between 72.83 and 488.27 W·m<sup>-2</sup>. The operating values in tests, such as refrigerant pressure and temperature, were taken in a built prototype. The numerical analysis was carried out considering different correlations proposed by Chen, Wojtan, and Kattan. The Wojtan mathematical model offered the best projection of the heat transfer effect for the different transition zones of a two-phase flow along the pipeline. The boiling heat transfer coefficients had approximate maximum values of 8.2, 8.5, 7.8, 6.7, and 5.8 kW·m<sup>-2</sup>·K<sup>-1</sup> for the A, B, C, D, and E tests prediction by Wojtan. Moreover, the boiling heat transfer coefficients increased as the mass velocity enhanced and the rise of vapor quality as the mass velocity was fixed. In this study, the effect of solar radiation, vapor quality on the measured heat transfer coefficient was analyzed.

**Keywords**— Heat transfer coefficient; hydrocarbon; fluid mechanics.

Manuscript received 9 Nov. 2020; revised 2 Mar. 2021; accepted 7 Apr. 2021. Date of publication 31 Aug. 2021.  
IJASEIT is licensed under a Creative Commons Attribution-Share Alike 4.0 International License.



### I. INTRODUCTION

Nowadays, the use of hydrocarbon refrigerants has become an environmentally friendly alternative [1]. The ecologically friendly refrigeration industry requires transitioning to working fluids with a low GWP and zero ODP energy-efficient [2]. According to Longo *et al.* [3] this type of refrigerant have an ozone-depleting potential (ODP) equal to 0 and a global warming potential (GWP) smaller than 3 [4]. Besides, their residence time in the atmosphere is less than one year [5]. Roy and Halder [6] mention that some developing nations have already adapted hydrocarbons by replacing Chlorofluorocarbons (CFC) and hydrofluorocarbons (HFC) as domestic refrigerant. Wu *et al.* [7] explain the negative impact of using conventional fluorinated refrigerants. Besides, they express that, since they are highly used as working fluids in heat pumps systems, their impact on the environment is manifested exponentially and produced a significant greenhouse effect when leaked.

Mehendale [8] develops a new correlation to predict the heat transfer coefficient of pure refrigerants and near-azeotropic refrigerant mixtures undergoing flow boiling within horizontal microfine tubes. The analysis includes vapor qualities from 0 to 1, heat and mass fluxes ranging from 1 to 58.7 kW·m<sup>-2</sup> and 25 to 820 kg·m<sup>-2</sup>·s<sup>-1</sup>. The new correlation performs better than any of the six selected correlations for the assessment in the 0.9–1.0 vapor quality range, the 50–100 kg·m<sup>-2</sup>·s<sup>-1</sup> mass flux range, saturation temperatures between –5 and 0 °C, and heat fluxes ranging from 0–5 and 50–55 kW·m<sup>-2</sup>.

Shao *et al.* [9] studied two-phase flow boiling of R134a in a pump-assisted separated heat pipe. A test section of 1 m effective length was prepared of the horizontal circular smooth copper tube with an inner diameter of 10 mm and outside diameter of 12 mm. The outside tube wall temperatures were measured by Pt1000 platinum resistance at five positions. The heat transfer coefficients were compared with the correlation given by Mohseni. It shows that all the

experimental data are inside the 10 % confidence interval predictions at  $x > 0.1$ . However, the error is 30% at  $x \leq 0.1$ .

Dang *et al.* [10] studied the flow boiling heat transfer characteristics for pure refrigerants of R134a, R245fa and their binary zeotropic mixture. The test plate consisted of seven parallel channel passages with the same total length of 110 mm and a cross-sectional area of  $2 \text{ mm}^2$ . The experiments were performed at the same inlet evaporating temperature of  $26 \text{ }^\circ\text{C}$  under conditions of the heat flux and mass flux ranging from 20 to  $350 \text{ kW}\cdot\text{m}^{-2}$  and 300 to  $400 \text{ kg}\cdot\text{m}^{-2}\cdot\text{s}^{-1}$ , respectively. The results indicated that the maximum heat transfer coefficient of R134a was  $27,000 \text{ W}\cdot\text{m}^{-2}\cdot\text{K}^{-1}$  while that for R245fa was  $18000 \text{ W}\cdot\text{m}^{-2}\cdot\text{K}^{-1}$ . Still, it decreased more severely when the heat transfer deterioration occurred at high heat flux.

Mostafa *et al.* [11] studied heat transfer in a matrix made up of five slotted tubes, using the refrigerant R290 as the working fluid. The experimental tests were taken with a constant saturation temperature of  $5.5 \text{ }^\circ\text{C}$ , a Reynolds number that varies between 200 and 2200, heat fluxes between 10 and  $40 \text{ kW}\cdot\text{m}^{-2}$  and flow rates between 100 and  $660 \text{ kg}\cdot\text{h}^{-1}$ . The results obtained based on R290 were compared with the refrigerant R134a and determined that the tube matrix's heat transfer coefficient is 25 % higher for R290 compared to R134a.

Sarmadian *et al.* [12] investigated the boiling heat transfer characteristics of the refrigerant isobutane (R600a). The tests were taken on a horizontal copper pipe with a length of 1000 mm and an internal diameter of 8.1 mm, in addition to the twisted interior tapes with torsion ratios of 4, 10 and 15, mass velocities of 160 to  $350 \text{ kg}\cdot\text{m}^{-2}\cdot\text{s}^{-1}$  and vapor qualities 0.1 to 0.8. The results showed that pipes with twisted tape present values in the heat transfer coefficient between 4500 and  $5500 \text{ W}\cdot\text{m}^{-2}\cdot\text{K}^{-1}$  and in a smooth pipe, the HTC is approximately  $3800 \text{ W}\cdot\text{m}^{-2}\cdot\text{K}^{-1}$  for a mass velocity of  $160 \text{ kg}\cdot\text{m}^{-2}\cdot\text{s}^{-1}$ , while, for a mass velocity of  $350 \text{ kg}\cdot\text{m}^{-2}\cdot\text{s}^{-1}$ , the pipes with twisted tape present an HTC between 8000 and  $10000 \text{ W}\cdot\text{m}^{-2}\cdot\text{K}^{-1}$ . For a smooth pipe, the HTC is presented with a value of approximately  $6000 \text{ W}\cdot\text{m}^{-2}\cdot\text{K}^{-1}$ , all the results for values in the steam quality between 0.55 and 0.8. Thus, concluding that the twisted tape increases heat transfer with increasing dough speed and steam quality.

The heat transfer characteristics by fluid boiling were studied by Choi *et al.* [13] for the refrigerant R290 in smooth horizontal microchannels with internal diameters of 1.5 and 3 mm. They applied working conditions such as heat flux, mass velocities, and saturation temperature of 5 to  $20 \text{ kW}\cdot\text{m}^{-2}$ , 50 to  $400 \text{ kg}\cdot\text{m}^{-2}\cdot\text{s}^{-1}$  and 0.5 and  $10 \text{ }^\circ\text{C}$ , respectively. They proved that the pipeline diameter is directly related to the interchange heat, where the heat transfer coefficient has a value of  $3500 \text{ W}\cdot\text{m}^{-2}\cdot\text{K}^{-1}$  for a diameter of 3 mm, and  $4500 \text{ W}\cdot\text{m}^{-2}\cdot\text{K}^{-1}$  for a diameter of 1.5 mm, for values of quality between 0.4 and 0.5. Similarly, the heat transfer coefficient takes values 4500, 4000, and  $3500 \text{ W}\cdot\text{m}^{-2}\cdot\text{K}^{-1}$  with saturation temperatures of 10, 5, and  $0 \text{ }^\circ\text{C}$ , respectively. The authors concluded that as the diameter decreases and the saturation temperature increases, the heat transfer coefficient increases and vice versa.

The present research aims to determine the heat transfer coefficients' behavior along a horizontal pipeline, using an ecological hydrocarbon refrigerant (R600a) and a renewable energy source (solar energy). For this purpose, five tests were

realized at different times, and the results will be shown using three other correlations proposed by Chen [14], Wojtan *et al.* [15] and Kattan *et al.* [16] which will have a different projection of the heat transfer coefficients.

## II. MATERIAL AND METHOD

Solar-assisted heat pumps (SAHP) operate under the use of the steam compression thermodynamic cycle [17]. This technology can convert and transport solar heat to the working fluid to store heat. With a size smaller than conventional heating systems, these systems may be able to capture the same amount of energy with a high percentage. Besides, they are suitable to operate at temperatures below  $70 \text{ }^\circ\text{C}$ ; this equipment can be equipped with photovoltaic panels [18]-[19]. According to Chatuverdi *et al.* [20], for the DX-SAHP system, the collector/evaporator is merged with a unit that seeks to transfer solar energy to the working fluid to demonstrate its effectiveness in saving energy, as shown in Fig. 1 [21]. Their applications include air conditioning, cold storage, solar drying, and water heating systems [22].

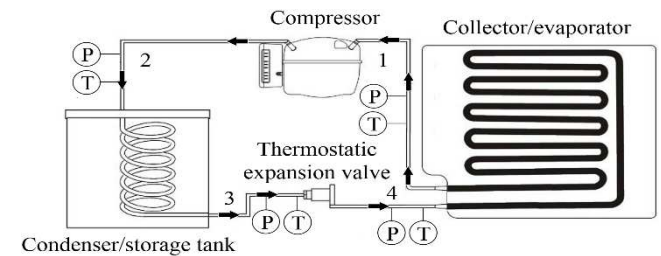


Fig. 1 DX-SAHP equipment used for obtaining experimental data [23].

### A. Collector/Evaporator

For the analysis of the heat transfer coefficients, we used initial data taken from the collector/evaporator shown in Fig. 2, which is part of a DX-SAHP system.

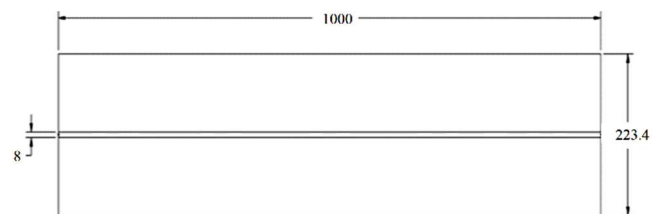


Fig. 2 Scheme of the collector/evaporator

Table 1 indicates physical data of the equipment that utilizes R600a refrigerant as working fluid.

TABLE I  
DATA OF THE FLAT-PLATE SOLAR COLLECTOR/EVAPORATOR

Variable	Value
Internal diameter	3.8 mm
External diameter	6.35 mm
Length of the pipeline	1000 mm
Area of the tube	$1.13411 \text{ E-5 m}^2$
Length of the collector	1000 mm
Width of the collector	223.4 mm
Cross-sectional area of the collector	$223400 \text{ mm}^2$

In the analysis, five tests were carried out at different times, obtaining the experimental data shown in Table 2, which

enable obtaining the heat transfer coefficients under different types of correlations.

TABLE II  
EXPERIMENTAL DATA FOR 5 DIFFERENT TESTS

Variables	A	B	C	D	E
Time	12:15	12:40	12:30	16:45	20:40
Ambient temperature [°C]	17.6	18.3	17.9	15.4	12
Average incident solar radiation [W·m <sup>-2</sup> ]	464.1	652.9	582.6	123.22	0
Mass flow [kg·s <sup>-1</sup> ]	0.002682	0.003031	0.002950	0.002602	0.002241
Quality	0.176	0.256	0.215	0.2305	0.2325
Surface temperature [°C]	14.5	14.5	14.5	12.6	9.5

### B. Correlations

From the study of the Chen [14], Kattan, *et al.* [16] and Wojtan *et al.* [15] correlations, a comparison between the three models is realized using the R600a refrigerant in horizontal pipelines, analyzing each of the flows that occur along the whole pipeline of the collector/evaporator.

The boiling heat transfer coefficient appears in both convective and nucleated forms. According to Saleem *et al.* [24], when the wall temperature exceeds the saturation temperature of a fluid by a certain degree, the transition from surface evaporation to nucleate boiling occurs. The nucleation produces steam bubbles that accumulate in the center of the tube, which causes the liquid to circulate close to the wall, producing an annular flow. It enables an increase in the liquid velocity so that the thin layer will continue to evaporate due to the nucleation. In contrast, the convective boiling appears at the liquid and steam interface with high values of quality, where the liquid film tends to dry in the superior part of the tube, and this benefit because the perimeter does not become wet.

1) *Correlation Proposed by Chen.* According to Chen [14] the total boiling heat transfer coefficient is obtained as the sum of its two forms, convective and nucleated, as indicated in equation 1.

$$h_{TP} = h_{nb} + h_{cb} \quad (1)$$

where  $h_{nb}$  is the nucleated heat transfer coefficient, and  $h_{cb}$  is the convective heat transfer coefficient. Chen [14] applies equations for two-phase flows, i.e., that both steam and liquid are present so that the convective heat transfer coefficient should be analyzed in the following way.

$$h_{cb} = 0.023 \left[ \frac{4m(1-x)}{\pi D \mu_L} \right]^{0.8} \left( \frac{\mu_L c_{pL}}{k_L} \right)^{0.4} \left( \frac{k_L}{D} \right) F \quad (2)$$

where the properties of the liquid are utilized since the heat is transferred by an annular film generated by the liquid and the wall, where  $F$  is the modification factor as a function of the Martinelli parameter ( $x_H$ ). On the other hand, the properties include the saturation temperature and pressure for the nucleated part. The temperature gradient keeps a relation with the flow rate and the steam quality.

$$h_{nb} = 0.00122 \left( \frac{k_L^{0.79} c_{pL}^{0.45} \rho_L^{0.49}}{\sigma^{0.5} \mu_L^{0.29} h_{LV}^{0.24} \rho_V^{0.24}} \right) \Delta T_{sat}^{0.24} \Delta P_{sat}^{0.75} S \quad (3)$$

where  $S$  is the suppression factor, applied to verify the experimental data, and it is represented with the two-phase Reynolds  $Re_{TP}$ .

2) *Correlation Proposed by Kattan et al:* Kattan *et al.* [16] propose a mathematical model that contains the boiling heat transfer coefficient, obtaining it from its convective and nucleated part. The total coefficient is analyzed depending on the flow zones that occur in the pipeline. If there are intermittent and annular zones, the dry angle will be equal to 0, but if different zones are found, the ratio with the stratified flow angle is considered.

$$\theta_{dry} = \theta_{strat} \frac{(G_{wavy} - G_A)}{(G_{wavy} - G_{strat})} \quad (4)$$

Afterwards, it is proceeded to determine the total boiling heat transfer coefficient, also known as the coefficient around the periphery.

$$h_{TP} = \frac{\theta_{dry} h_v + (2\pi - \theta_{dry}) h_{wet}}{2\pi} \quad (5)$$

The heat transfer coefficient in the vapor phase is determined by applying equation 6, obtaining its parameters from the temperature at the evaporator's outlet and with steam quality equal to 1.

$$h_v = 0.023 \left( \frac{G_A x D}{\alpha \mu_v} \right)^{0.8} \left( \frac{c_{pv} \mu_v}{k_v} \right)^{0.4} \frac{k_v}{D} \quad (6)$$

The liquid phase's heat transfer coefficient includes the nucleated and convective boiling analysis, as shown in equation 7.

$$h_{wet} = [(h_{cb})^3 + (h_{nb})^3]^{\frac{1}{3}} \quad (7)$$

where  $h_{cb}$  presents the convective boiling constant and the exponent of the Reynolds number with values 0.0133 and 0.69, respectively, used in equation 8. The thickness  $\delta$  of the liquid film, with the liquid Reynolds number  $Re_L$ , considers the liquid part properties since they have the same concept as Chen [14].

$$h_{cb} = C Re_L^m Pr_L^{0.4} \frac{k_L}{\delta} \quad (8)$$

$$\delta = \frac{\pi D (1-\alpha)}{2(2\pi - \theta_{dry})} \quad (9)$$

$$Re_L = \frac{4G_A(1-x)\delta}{(1-\alpha)\mu_L} \quad (10)$$

The film's thickness considers a different analysis in the dry angle compared to in equation 9, using the following equation 11.

$$\theta_{dry} = \theta_{strat} \quad (11)$$

The  $h_{nb}$  uses a reduced pressure  $P_{re}$ , the molecular weight of the fluid  $M$  and the heat flux, where it is taken into account the roughness of the surface equivalent to one micron. Still, Kattan *et al.* [16] assume it is not necessary when performing the calculations. At the same time, they indicate that this nucleate boiling coefficient is aimed at predicting the value of using the refrigerants.

$$h_{nb} = 55(P_{re})^{0.12}(-\log \cdot P_{re})^{-0.55}M^{-0.5}\left(\dot{q}\right)^{0.67} \quad (12)$$

3) *Correlation proposed by Wojtan et al.*: Wojtan *et al.* [15] proposed an improvement to the correlation proposed by Kattan *et al.* [16], which includes in the analysis more zones that may be present in the pipeline. For this purpose, the authors propose to study the dry angle for the different zones that can be found in the flow patterns along a pipe, where the stratified angle will be equal to 0 when finding zones such as slug, intermittent and annular. Equation 13 will be used for dry out and mist zones, while for areas such as slug + stratified-wavy, equation 14 will be used.

$$\theta_{dry} = \theta_{strat} \frac{(G_{wavy} - G_A)}{(G_{wavy} - G_{strat})} \quad (13)$$

$$\theta_{dry} = \left[ \frac{(G_{wavy} - G_A)}{(G_{wavy} - G_{strat})} \right]^{0.61} \theta_{strat} \quad (14)$$

On the other hand, equation 5 allows the calculation of the two-phase heat transfer coefficient  $h_{TP}$  and equation 6 the heat transfer coefficient in the vapor zone or the drying perimeter  $h_v$ . In contrast, equation 7 is used for the coefficient of heat transfer in the zone of liquid or humid perimeter  $h_{wet}$ , which are the same of Kattan *et al.* [16]. However, as it is known, the latter uses  $h_{cb}$  and  $h_{nb}$  from equations 8 and 12 and the same aforementioned analysis; the only difference is that for nucleated boiling, Wojtan *et al.* [15] multiply by a factor  $S$  of 0.8, which helps to predict the experimental points with more accuracy, especially for higher heat flux and for convective boiling. The thickness of the film  $\delta$  takes into account equation 15 for its analysis, indicating the update of the model.

$$\delta = \frac{D}{2} - \sqrt{\left(\frac{D}{2}\right)^2 - \frac{2A_L}{(2\pi - \theta_{dry})}} \quad (15)$$

where the drying angle will be replaced by the stratified angle, as shown in equation 16:

$$\theta_{dry} = \theta_{strat} \quad (16)$$

where  $A_L$  is the cross-sectional area of the liquid, as indicated in equation 17.

$$A_L = 0.5R^2[(2\pi - \theta_{strat}) - \sin(2\pi - \theta_{strat})] \quad (17)$$

Another difference in this improvement is in the mist's analysis, dry out and stratified-wavy zones. If a dry out zone is present, equation 18 is specifically utilized for the dry out zone instead of using  $h_{TP}$ .

$$h_{dryout} = h_{tp}(x_{di}) \quad (18)$$

where  $x_{di}$  is the quality at the beginning of the dry out zone, from the Weber and Froude number for the vapor zone.

$$x_{di} = 0.58e^{\left[0.52 - 0.235We_v^{0.17}Fr_v^{0.37}\left(\frac{\rho_v}{\rho_L}\right)^{0.25}\left(\frac{q}{q_{crit}}\right)^{0.70}\right]} \quad (19)$$

$$We_v = \frac{G_A^2 D}{\rho_v \sigma} \quad (20)$$

$$Fr_v = \frac{G_A^2}{[gD\rho_v(\rho_L - \rho_v)]} \quad (21)$$

Such analysis is only performed when the dry-out zone is present, while in the mist zone is present, the analysis varies with the use of a homogeneous Reynolds ( $Re_H$ ) and a multiplying factor  $Y$ , obtained as follows:

$$h_{mist} = 0.0117Re_H^{0.79}Pr_v^{1.06}Y^{-1.83}\frac{k_v}{D} \quad (22)$$

$$Re_H = \frac{G_A D}{\mu_v} \left[ x + \frac{\rho_v}{\rho_L} (1 - x) \right] \quad (23)$$

$$Y = 1 - 0.1 \left[ \left( \frac{\rho_L}{\rho_v} - 1 \right) (1 - x) \right] \quad (24)$$

Indeed, the heat transfer coefficient for the dry out zone changes, inserting the coefficient of the mist zone, as follows:

$$h_{dryout} = h_{TP}(x_{di}) - \frac{x - x_{di}}{x_{de} - x_{di}} [h_{TP}(x_{di}) - h_{mist}(x_{de})] \quad (25)$$

where  $x_{de}$  is the dry out completion quality, which is obtained from equation 26.

$$x_{de} = 0.61e^{\left[0.57 - 5.8 \cdot 10^{-3}We_v^{0.38}Fr_v^{0.15}\left(\frac{\rho_v}{\rho_L}\right)^{-0.09}\left(\frac{q}{q_{crit}}\right)^{0.27}\right]} \quad (26)$$

The analysis suggested by Wojtan *et al.* [15] to determine the boiling heat transfer coefficient identifies in a better manner the zones present in the pipeline since it enables to see the start of the dry out or the mist.

### III. RESULTS AND DISCUSSION

Various tests were carried out at different times to obtain the results, for which the correlations mentioned in the previous section were utilized. The plots showed a similar trend to the ones presented by Chen [14], Wojtan *et al.* [15] and Kattan *et al.* [16].

#### A. Test A

Fig. 3 shows three heat transfer coefficients obtained in tests realized at 12:15 with an incident solar radiation of  $464.1 \text{ W}\cdot\text{m}^{-2}$  [23]. The curves show an increasing trend from their initial point up to a quality value greater than 0.9, but when in the dry out zone, the three curves have the same behavior decreasing in an accelerated manner to values between 4 and  $5 \text{ kW}\cdot\text{m}^{-2}\cdot\text{K}^{-1}$ , respectively.

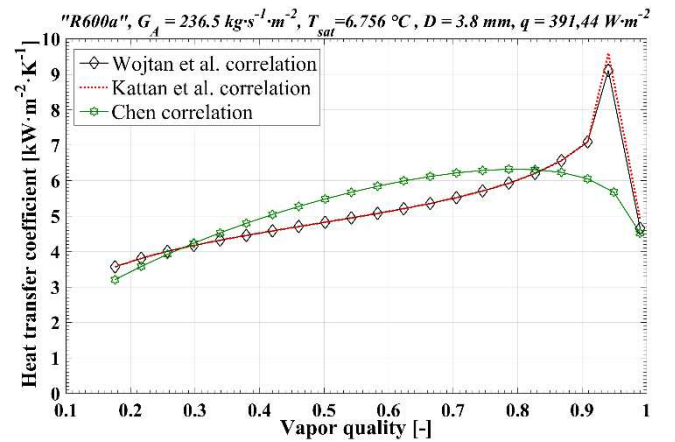


Fig. 3 Heat transfer coefficient with initial quality 0.176

### B. Test B

For case B shown in Fig. 4, tests were carried out with experimental data taken at 12:40, where the incident solar radiation had a maximum value of  $659.2 \text{ W}\cdot\text{m}^{-2}$ . The curves take a trend upward at the initial values of quality until reaching an approximate value of 0.9, where the curve drops in an accelerated manner for the Chen [14] and Kattan *et al.* [16] correlations until reaching values of  $4.5$  and  $6 \text{ kW}\cdot\text{m}^{-2}\cdot\text{K}^{-1}$ , respectively, while the heat transfer coefficient descended to values smaller than  $1 \text{ kW}\cdot\text{m}^{-2}\cdot\text{K}^{-1}$  for the Wojtan *et al.* [15] correlation.

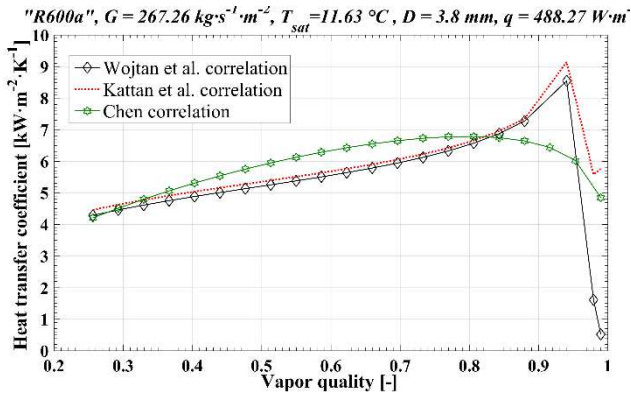


Fig. 4 Heat transfer coefficient with initial quality 0.256

### C. Test C

Fig. 5 shows the heat transfer coefficients obtained using experimental data taken at 12:30, with an incident solar radiation of  $582.6 \text{ W}\cdot\text{m}^{-2}$  [23]. The plot shows the heat transfer coefficient's real behavior within the tube, with a curve increasing from the initial values of quality and an accelerated drop when reaching quality values greater than 0.9. For the Chen [14] and Kattan *et al.* [16] correlations, during the drop, the values fluctuate between  $4.5$  and  $6 \text{ kW}\cdot\text{m}^{-2}\cdot\text{K}^{-1}$ , respectively, while for the Wojtan *et al.* [15] correlation, it descended to values smaller than  $1 \text{ kW}\cdot\text{m}^{-2}\cdot\text{K}^{-1}$ .

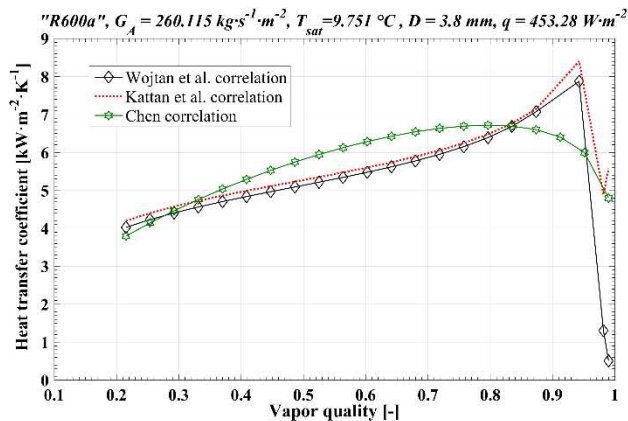


Fig. 5 Heat transfer coefficient with initial quality 0.215

The coefficients obtained from the Kattan *et al.* [16] model for tests B and C shown in Fig. 4 and 5, respectively, indicate a behavior similar to the Wojtan *et al.* [15] model; when showing a minimum zone of mist flow, the tests tend to increase from their limit with the dry-out zone, due to the lack of analysis for such zone. The Wojtan *et al.* [15] mathematical model provides a more accurate prediction of the heat transfer coefficient depending on the zones where the flow is found.

The behavior is similar for tests B and C, obtaining minimum heat transfer values of  $0.516$  and  $0.507 \text{ kW}\cdot\text{m}^{-2}\cdot\text{K}^{-1}$ , respectively. Equations 22 to 26 are used to get the predictions shown in Fig. 4 and 5, which show the final behavior of the heat transfer coefficient.

### D. Test D

The heat transfer coefficients for experiment D are presented in Fig. 6, which were obtained with experimental data taken at 16:45, with an incident solar radiation of  $123.22 \text{ W}\cdot\text{m}^{-2}$  [23].

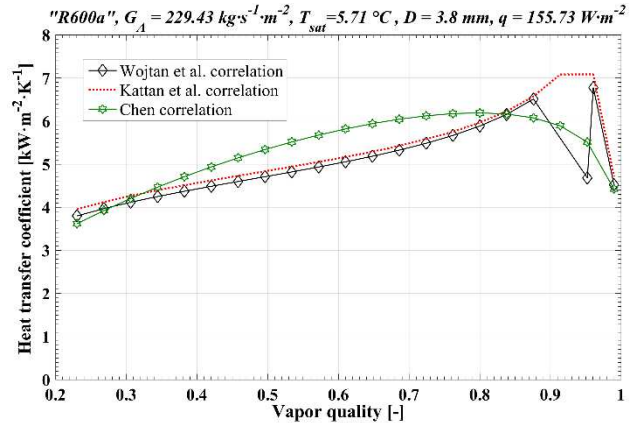


Fig. 6 Heat transfer coefficient with initial quality 0.2305

The plots show a similar trend, with growth for the initial values of quality and an accelerated drop to values between  $4$  and  $5 \text{ kW}\cdot\text{m}^{-2}\cdot\text{K}^{-1}$  for values of quality greater than  $0.85$ , with different behavior respects Wojtan *et al.* [15] correlation.

### E. Test E

Fig. 7 indicates the heat transfer coefficients obtained with experimental data taken at 20:40, with an incident solar radiation of  $0 \text{ W}\cdot\text{m}^{-2}$ . The plots show an increasing behavior from the initial values of quality up to  $0.85$  quality, where the plot decreases to values between  $3.5$  and  $5 \text{ kW}\cdot\text{m}^{-2}\cdot\text{K}^{-1}$ ; there is different behavior in the plot Wojtan *et al.* [15] correlation.

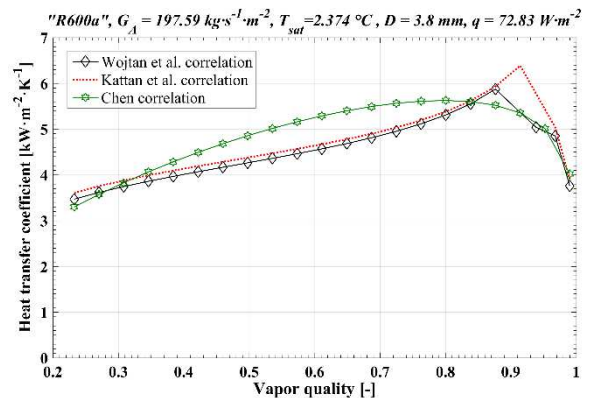


Fig. 7 Heat transfer coefficient with initial quality 0.2325

Fig. 6 and 7 corresponded to tests D and E, the plot has a prediction different from the other plots for the Wojtan *et al.* [15] correlation since, due to the zone change of the flow, the model performs a different analysis for the dry out angle; when a stratified-wavy zone is present, the correlation specifies the use of equation 18. This zone's behavior is a drop and then an ascending trend in the heat transfer coefficient,

which tends to decrease when finding the dry-out zone, as shown in most of the cases.

### F. Effect of the Heat Flux and Mass Velocity

The three models studied for the different tests realized are shown in Fig. 8, 9, and 10, where it presents for the highest values of heat flux and mass velocities of 488.27 W·m<sup>-2</sup> and 267.26 kg·m<sup>-2</sup>·s<sup>-1</sup>, respectively, the heat transfer coefficients will be larger, while for the smallest values of heat flux and mass velocities of 72.83 W·m<sup>-2</sup> and 197.59 kg·m<sup>-2</sup>·s<sup>-1</sup>, respectively, the heat transfer coefficients will be smaller.

Chen [14] correlation shown in Fig. 8 indicates a general investigation of the heat transfer coefficient along a pipeline without analyzing the different zones' behavior where there is two-phase flow. Furthermore, the model of Kattan *et al.* [16], shown in Fig. 9, presents an updated study of the heat transfer coefficient; their analysis indicates an exponential trend in the plot. Additionally, the value tends to drop in an accelerated manner when exceeding the quality of 0.9 and to find a different zone in the two-phase flow distribution. Wojtan *et al.* [15] obtained an updated correlation after finding three new zones for flow patterns. The new correlation shown in Fig. 10 presents an analysis about the behavior of the heat transfer coefficient, which indicates that when finding zones such as mist, the trend of the plot will drop to values smaller than 1 kW·m<sup>-2</sup>·K<sup>-1</sup>, while for zones such as stratified-wavy, it will show an exponential trend of drop and growth until reaching the dry-out zone.

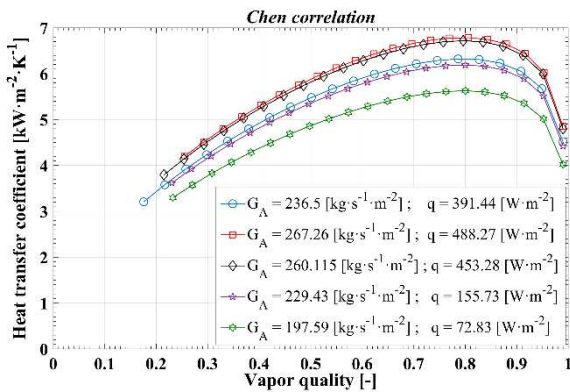


Fig. 8 Chen [14] correlation for different heat flows and mass velocities.

Kattan *et al.* [16] correlation show an updated calculation about the heat transfer coefficients, reducing the iterative calculations and studying the behavior of a two-phase flow within the pipeline in a more precise manner. However, even then, the correlation does not show the heat transfer coefficients' actual behavior because not all the zones that occur in the boiling process of a pipeline are studied. Wojtan *et al.* [15] modified the Kattan *et al.* [16] correlate and show equations that eliminate iterative calculations to precisely analyze a boiling fluid's behavior. Their analysis extends for the three new zones found: slug, slug + stratified-wavy, and stratified-wavy, and explain that a distinct behavior of the heat transfer coefficient exists in each zone, as can be distinguished in Fig. 4, 5, 6, and 7.

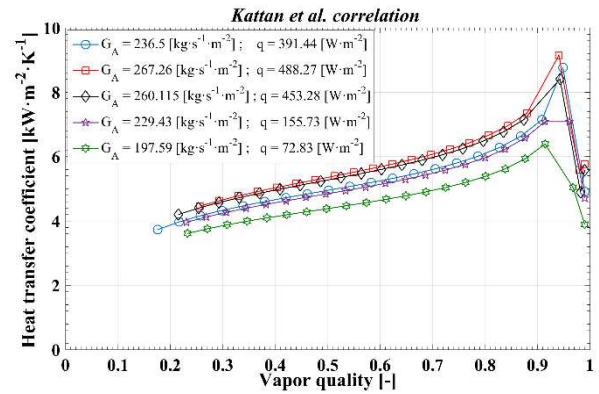


Fig. 9 Kattan *et al.* [16] correlation for distinct heat flows and mass velocities.

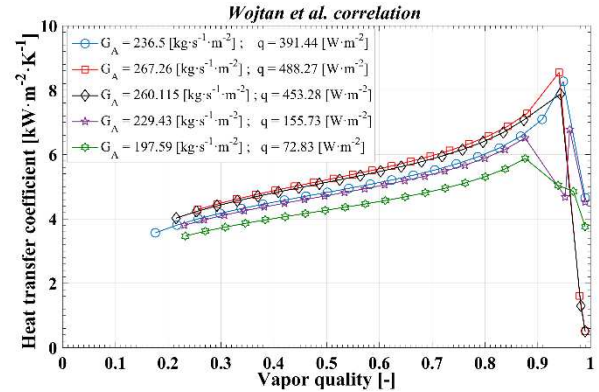


Fig. 10 Wojtan *et al.* [15] correlation for distinct heat flows and mass velocities.

## IV. CONCLUSION

The use of hydrocarbons such as R600a and R290 has become a clear alternative for replacing conventional refrigerants such as R22 for refrigeration systems and DX-SAHP systems. The heat transfer coefficients were investigated in a collector/evaporator with a horizontal copper pipeline with an internal diameter of 3.8 mm, for distinct heat flux and mass velocities. Based on three different models, the results indicated the following:

- Heat flux and mass velocity are directly proportional to the heat transfer coefficient since they have 488.27 and 267.26, respectively. Applying Chen [14], Kattan *et al.* [16], and Wojtan *et al.* [15] models, maximum values of 6.78, 9.15, and 8.55 kW·m<sup>-2</sup>·K<sup>-1</sup>, respectively, were obtained.
- When a general study about the heat transfer coefficient is realized, like the one performed by Chen [14], the plot showed a growing trend for approximate values up to 0.8, and it will drop to minimum values between 4 and 5 kW·m<sup>-2</sup>·K<sup>-1</sup> when this quality limit is exceeded.
- The best results were obtained employing test A; the three models start at values between 3 and 4 kW·m<sup>-2</sup>·K<sup>-1</sup> for an initial quality value of 0.176, and end at approximate values between 4 and 5 kW·m<sup>-2</sup>·K<sup>-1</sup> for maximum quality of 0.99.

## NOMENCLATURE

$A_L$	Cross-sectional area of the liquid	m <sup>2</sup>
$C$	Constant	-
$C_p$	Specific heat at constant pressure	J·kg <sup>-1</sup> ·K <sup>-1</sup>

$D$	Inner diameter	m
$F$	Modification factor	-
$Fr$	Froude number	-
$g$	Gravity	$\text{m}\cdot\text{s}^{-2}$
$\dot{G}_A$	Mass velocity	$\text{kg}\cdot\text{m}^{-2}\cdot\text{s}^{-1}$
$h_{iv}$	Enthalpy vaporization	$\text{J}\cdot\text{kg}^{-1}$
$h_{TP}$	Two-phase heat transfer coefficient	$\text{W}\cdot\text{m}^{-2}\cdot\text{K}^{-1}$
$h_{nb}$	Nucleated heat transfer coefficient	$\text{W}\cdot\text{m}^{-2}\cdot\text{K}^{-1}$
$h_{cb}$	Convective heat transfer coefficient	$\text{W}\cdot\text{m}^{-2}\cdot\text{K}^{-1}$
$h_{wet}$	Liquid heat transfer coefficient	$\text{W}\cdot\text{m}^{-2}\cdot\text{K}^{-1}$
$k$	Thermal conductivity	$\text{W}\cdot\text{m}^{-1}\cdot\text{K}^{-1}$
$m$	Mass flow	$\text{kg}\cdot\text{s}^{-1}$
$M$	Molar mass	$\text{g}\cdot\text{mol}^{-1}$
$P$	Pressure	kPa
$Pr$	Prandtl number	-
$P_{re}$	Reduced pressure	-
$q$	Heat flux	$\text{W}\cdot\text{m}^{-2}$
$q_{crit}$	Critical heat flux	$\text{W}\cdot\text{m}^{-2}$
$R$	Inner radius	m
$Re$	Reynolds number	-
$Re_H$	homogeneous reynolds number	-
$Re_{TP}$	Two-phase Reynolds number	-
$S$	Suppression factor	-
$T$	Temperature	K
$We$	Weber number	-
$x$	Vapor quality	-
$x_{di}$	Quality at the beginning of the dryout zone	-
$x_{de}$	Dryout completion quality	-
$Y$	multiplying factor	-

#### Greek letters

$\mu$	Dynamic viscosity	$\text{kg}\cdot\text{m}^{-1}\cdot\text{s}^{-1}$
$\sigma$	Surface tension	$\text{N}\cdot\text{m}^{-1}$
$\rho$	Density	$\text{kg}\cdot\text{m}^{-3}$
$\theta$	Angle	rad
$\alpha$	Void fraction	-
$\delta$	thickness of the film	m

#### Subscripts

$dry$	Dryout zone
$L$	Liquid phase
$v$	Vapor phase
$sat$	Saturation
$strat$	Stratified zone
$wavy$	Wavy zone

#### ACKNOWLEDGMENT

The authors are grateful to the Renewable Energies and Mechanical Implementation of SMEs Research Group (GIERIMP), Universidad Politécnica Salesiana and Universidad Pontificia Bolivariana

#### REFERENCES

- [1] D. Calleja-Anta, L. Nebot-Andrés, J. Catalán-Gil, D. Sánchez, R. Cabello, and R. Llopis, "Thermodynamic screening of alternative refrigerants for R290 and R600a," *Results Eng.*, vol. 5, p. 100081, Mar. 2020, doi: 10.1016/j.rineng.2019.100081.
- [2] E. Allymeh, Á. Á. Pardiñas, T. M. Eikevik, and A. Hafner, "Comparative analysis of evaporation of isobutane (R600a) and propylene (R1270) in compact smooth and microfinned tubes," *Appl. Therm. Eng.*, vol. 188, p. 116606, Apr. 2021, doi: 10.1016/j.applthermaleng.2021.116606.
- [3] G. A. Longo, S. Mancin, G. Righetti, C. Zilio, and J. Steven Brown, "Assessment of the low-GWP refrigerants R600a, R1234ze(Z) and R1233zd(E) for heat pump and organic Rankine cycle applications," *Appl. Therm. Eng.*, vol. 167, p. 114804, Feb. 2020, doi: 10.1016/j.applthermaleng.2019.114804.
- [4] S. C. Yelishala, K. Kannaiyan, R. Sadr, Z. Wang, Y. A. Levendis, and H. Metghalchi, "Performance maximization by temperature glide matching in energy exchangers of cooling systems operating with natural hydrocarbon/CO2 refrigerants," *Int. J. Refrig.*, vol. 119, pp. 294–304, Nov. 2020, doi: 10.1016/j.ijrefrig.2020.08.006.
- [5] D. V. Raghunatha Reddy, P. Bhrmara, and K. Govindarajulu, "A Comparative Study of Multiple Regression and Artificial Neural Network models for a domestic refrigeration system with a hydrocarbon refrigerant mixtures," in *Materials Today: Proceedings*, 2019, vol. 22, pp. 1545–1553, doi: 10.1016/j.matpr.2020.02.116.
- [6] Z. Roy and G. Halder, "Replacement of halogenated refrigerants towards sustainable cooling system: A review," *Chem. Eng. J. Adv.*, vol. 3, p. 100027, Nov. 2020, doi: 10.1016/j.ceja.2020.100027.
- [7] D. Wu, B. Hu, and R. Z. Wang, "Vapor compression heat pumps with pure Low-GWP refrigerants," *Renewable and Sustainable Energy Reviews*, vol. 138, Elsevier Ltd, p. 110571, 01-Mar-2021, doi: 10.1016/j.rser.2020.110571.
- [8] S. Mehendale, "A new heat transfer coefficient correlation for pure refrigerants and near-azeotropic refrigerant mixtures flow boiling within horizontal microfin tubes," *Int. J. Refrig.*, vol. 86, pp. 292–311, Feb. 2018, doi: 10.1016/j.ijrefrig.2017.11.017.
- [9] J. Shao, X. Li, Z. Guo, T. Ma, R. Liu, and X. Tian, "Flow pattern, pressure drop and heat transfer coefficient during two-phase flow boiling of R134a in pump-assisted separate heat pipe," *Exp. Therm. Fluid Sci.*, vol. 85, pp. 240–247, Jul. 2017, doi: 10.1016/j.expthermflusci.2017.03.007.
- [10] C. Dang, L. Jia, Q. Peng, L. Yin, and Z. Qi, "Experimental study on flow boiling heat transfer for pure and zeotropic refrigerants in multi-microchannels with segmented configurations," *Int. J. Heat Mass Transf.*, vol. 127, pp. 758–768, Dec. 2018, doi: 10.1016/j.ijheatmasstransfer.2018.08.083.
- [11] I. Mostafa, P. H. Jin, Z. Zhang, and W. Q. Tao, "Experimental study of the falling film evaporation coefficients of R290 in a horizontal enhanced tube array," *Int. J. Heat Mass Transf.*, vol. 159, p. 120099, Oct. 2020, doi: 10.1016/j.ijheatmasstransfer.2020.120099.
- [12] A. Sarmadian *et al.*, "Flow boiling heat transfer and pressure drop characteristics of Isobutane in horizontal channels with twisted tapes," *Int. J. Heat Mass Transf.*, vol. 162, p. 120345, Dec. 2020, doi: 10.1016/j.ijheatmasstransfer.2020.120345.
- [13] K. H. Choi, A. S. Pamitran, J. T. Oh, and K. Saito, "Pressure drop and heat transfer during two-phase flow vaporization of propane in horizontal smooth minichannels," *Int. J. Refrig.*, vol. 32, no. 5, pp. 837–845, Aug. 2009, doi: 10.1016/j.ijrefrig.2008.12.005.
- [14] J. C. Chen, "Correlation for Boiling Heat Transfer to Saturated Fluids in Convective Flow," *Ind. Eng. Chem. Process Des. Dev.*, vol. 5, no. 3, pp. 322–329, Jul. 1966, doi: 10.1021/i260019a023.
- [15] L. Wojtan, T. Ursenbacher, and J. R. Thome, "Investigation of flow boiling in horizontal tubes: Part II - Development of a new heat transfer model for stratified-wavy, dryout and mist flow regimes," *Int. J. Heat Mass Transf.*, vol. 48, no. 14, pp. 2970–2985, Jul. 2005, doi: 10.1016/j.ijheatmasstransfer.2004.12.013.
- [16] N. Kattan, J. R. Thome, and D. Favrat, "Flow Boiling in Horizontal Tubes: Part 3—Development of a New Heat Transfer Model Based on Flow Pattern," *J. Heat Transfer*, vol. 120, no. 1, pp. 156–165, Feb. 1998, doi: 10.1115/1.2830039.
- [17] C. A. Isaza-Roldan, W. Quitiaquez, C. Nieto-Londoño, L. Toapanta, and I. Simbaña, "Alternative energy storage using a domestic hot water solar-assisted heat pump with PV collector/evaporator and HC refrigerant," in *ICR 2019 - 25th IIR International Congress of Refrigeration*, 2019, pp. 4827–4839, doi: 10.18462/iir.icr.2019.1537.
- [18] F. Martorana, M. Bonomolo, G. Leone, F. Monteleone, G. Zizzo, and M. Beccali, "Solar-assisted heat pumps systems for domestic hot water production in small energy communities," *Sol. Energy*, vol. 217, pp. 113–133, Mar. 2021, doi: 10.1016/j.solener.2021.01.020.
- [19] A. Badieli *et al.*, "A chronological review of advances in solar assisted heat pump technology in 21st century," *Renewable and Sustainable Energy Reviews*, vol. 132, Elsevier Ltd, p. 110132, 01-Oct-2020, doi: 10.1016/j.rser.2020.110132.
- [20] S. K. Chaturvedi, V. D. Gagrani, and T. M. Abdel-Salam, "Solar-assisted heat pump - A sustainable system for low-temperature water

- heating applications," *Energy Convers. Manag.*, vol. 77, pp. 550–557, Jan. 2014, doi: 10.1016/j.enconman.2013.09.050.
- [21] E. Mohamed, S. Riffat, S. Omer, and R. Zeinelabdien, "A comprehensive investigation of using mutual air and water heating in multi-functional DX-SAMHP for moderate cold climate," *Renew. Energy*, vol. 130, pp. 582–600, Jan. 2019, doi: 10.1016/j.renene.2018.06.075.
- [22] W. Ji, J. Cai, J. Ji, and W. Huang, "Experimental study of a direct expansion solar-assisted heat pump (DX-SAHP) with finned-tube evaporator and comparison with conventional DX-SAHP," *Energy Build.*, vol. 207, p. 109632, Jan. 2020, doi: 10.1016/j.enbuild.2019.109632.
- [23] W. Quitiaquez, I. Simbaña, C. A. Isaza-Roldán, C. Nieto-Londoño, P. Quitiaquez, and L. Toapanta-Ramos, "Performance Analysis of a Direct-Expansion Solar-Assisted Heat Pump Using a Photovoltaic/Thermal System for Water Heating BT - Smart Technologies, Systems and Applications," 2020, pp. 89–102.
- [24] A. Saleem, S. Farooq, I. A. Karimi, and R. Banerjee, "Wall superheat at the incipient nucleate boiling condition for natural and forced convection: A CFD approach," *Comput. Chem. Eng.*, vol. 134, p. 106718, Mar. 2020, doi: 10.1016/j.compchemeng.2019.106718.